Theor. Appl. Climatol. 83, 169–179 (2006)
DOI 10.1007/s00704-005-0137-0

Theoretical and Applied Climatology
Printed in Austria

Department of Applied Climatology and Landscape Ecology, Institute of Geography,
University of Duisburg-Essen, Campus Essen, Essen, Germany

Comparison of in-situ measured ground heat fluxes within a heteorogeneous urban ballast layer

S. Weber

With 6 Figures

Received June 1, 2004; revised February 10, 2005; accepted February 16, 2005
Published online July 22, 2005

Summary

This study concentrates on measurements of ground heat fluxes within a porous urban ballast layer that were conducted from June to September 2002 at the goods station in Osnabrück, Germany. To account for the limitation of accurately installing sensors within the heterogeneous and porous ballast bulk, the heat fluxes were calculated from four different methods to compare their variability, dynamics and shortcomings. Ground heat fluxes were gathered from 1) a heat flux plate with the inclusion of heat storage between the soil surface and the heat flux plate, 2) temperature gradient measurements with correction for heat storage, 3) temperature gradient measurements with a modelled surface temperature and a laboratory derived thermal conductivity, 4) as residual from the surface energy balance equation. The results show a distinct deviation of the four methods for absolute values of the ground heat flux as well as for temporal dynamics on the diurnal cycle. As indicated by the temporal dynamics of the ground heat flux times series and a simple error analysis of the four methods, the most plausible estimates for an urban application in a heterogeneous ballast layer were obtained by temperature gradient measurements between the surface and −0.05 m. Overall, the results indicate that accurate ground heat flux measurements in urban applications still prove difficult to acquire.

1. Introduction

Due to the generally smaller magnitude of ground heat flux (Q_G) compared to the other energy fluxes the determination of this flux in energy-balance studies at the earth's surface is often handled rather simply, e.g. by parameterising Q_G as a constant fraction of the net radiation. However, this is not suitable for specific surfaces such as bare soil, non-natural materials or urban surfaces where Q_G is a dominant part of the energy budget and can amount to more than 50% of the net radiation (e.g. Oke et al., 1999; Jauregui et al., 2002).

Specific attention has to be paid when studying urban ground heat fluxes. Two scenarios have to be considered: First, the measurement of local scale Q_G for an urban volume, e.g. in urban energy balance studies or, second, Q_G measurements of an isolated urban facet. Both scenarios face methodological limitations. Due to the complex three-dimensional structure of the urban area in the local scale, more than one active surface in the flux footprint may have to be considered when estimating Q_G (e.g. roofs, ground and walls within street canyons). Therefore, a storage heat flux term (ΔQ_S) was introduced in urban applications which defines the net heat change in the urban volume below measurement height taking into account the urban canopy air layer, buildings, vegetation and the ground (Oke, 1988; Grimmond and Oke, 1999). However, since it

proves difficult to evaluate ΔQ_S experimentally in an urban area it is set equal to Q_G in most studies. Q_G is then parameterised as a fraction of the net radiation Q^* or by determining it as the residual term in the surface energy-balance equation (Oke et al., 1999; Spronken-Smith, 2002; Christen and Vogt, 2004). Since both methods tend to introduce inaccuracies e.g. by closure gaps within the energy-balance-equation, they are still not satisfactory. Some progress may be achieved by approaches to model the storage heat flux which have improved greatly during recent years (e.g. Roth and Oke, 1994; Grimmond and Oke, 2002; Masson et al., 2002; Roberts et al., 2003).

If the intention is to measure the ground heat flux of a horizontal urban facet at a smaller scale e.g. of a road or a parking lot, limitations may arise due to the complexity of urban building materials and the problems associated with inaccurately installed sensors. Studies reporting from in-situ measurements within different urban and non-natural surface materials like asphalt (Asaeda et al., 1996; Anandakumar, 1999), concrete (Doll et al., 1985), gravel (Al-Turki et al., 1997), macadam and sand (Asaeda et al., 1996) encounter similar problems relating to the installation of sensors within these materials. Heat flux plates (HFP) are prone to measurement errors which are associated with deviation of the plate thermal conductivity to the material conductivity, poor contact of the plate and the substrate and blocking vertical heat and water transport within the substrate (Mogensen, 1970; Watts et al., 1990; van Loon et al., 1998; Sauer, 2002; Sauer et al., 2003). Physical contact between the HFP and the substrate is believed to decrease with increasing grain size of the substrate leading to increasing cavities between grains. Since the HFP is normally buried at some depth beneath the surface the heat storage in the layer above the plate has to be accounted for which requires sufficient knowledge of the soil thermal properties (Mayocchi and Bristow, 1995; Kukharets et al., 1998). Temperature sensors (thermocouples, Pt100, thermistors) might be subject to poor contact with the material, especially when measuring in solid or highly porous materials (e.g. Doll et al., 1985).

This brief overview outlines that in-situ measurements are, to a certain degree, prone to methodological and technical limitations. The main problem is that there is no standard to which urban Q_G measurements can be calibrated (Roberts et al., 2003).

The intention of this study was to measure Q_G of an isolated urban facet with different in-situ and residual approaches and compare the variability, dynamics and shortcomings of the methods. The measurements were conducted within the framework of a study on the energy-balance and cold-air dynamics within an urban environment (Weber and Kuttler, 2003, 2004).

After the theoretical background is briefly outlined (Section 2), the site and instrumentation as well as the methods used to calculate Q_G are described in Section 3. Results concerning ballast thermal properties and Q_G measurements are given (Section 4) and differences in absolute magnitude of Q_G as well as in temporal dynamics on the daily cycle between the different methods are compared.

2. Theoretical background

The heat flux into the ground can be calculated by Fourier's law of heat conduction as

$$Q_G = \lambda \frac{\partial T}{\partial z} \tag{1}$$

with Q_G the ground heat flux in $W\,m^{-2}$, λ the thermal conductivity in $W\,m^{-1}\,K^{-1}$ and $\partial T/\partial z$ the ground temperature gradient in $K\,m^{-1}$. In practical applications the differential quotient is usually substituted by a difference quotient owing to only a few discrete measurement locations within the ground.

A heat flux plate that is buried at some depth within the substrate does not represent the true heat flux at the surface because of the flux divergence $\partial Q_G/\partial z$ within the soil. Since the surface energy-balance equation refers to the ground surface at $z = 0\,m$ the heat flux at the surface must be written as

$$Q_G = Q_{G(z)} + Q_S \tag{2}$$

with $Q_{G(z)}$ the ground heat flux at the depth z the HFP is buried and Q_S the heat storage in the layer above the HFP, all in $W\,m^{-2}$ (Arya, 2001).

The term Q_S can be evaluated calorimetrically (Sauer, 2002)

$$Q_S = \int_z^0 C_v \frac{\partial T}{\partial t} \partial z \quad (3)$$

with C_v the volumetric heat capacity in $J\,m^{-3}\,K^{-1}$, $\partial T/\partial t$ the time rate of change of the layer-averaged temperature in the layer above the HFP in $K\,s^{-1}$ and ∂z the layer thickness in m. Coupling of the gradient- or HFP-method with a calorimetric approach is usually referred to in the literature as the ''combination method'' (Sauer, 2002).

3. Material and methods

3.1 Site characteristics and ballast physical properties

Measurements were carried out at the goods station (GS) in the city of Osnabrück, Germany (52° 16′ N, 8° 04′ E). The ballast surface at the goods station covers a surface area of approximately $0.5\,km^2$. The GS is bounded by the city centre of Osnabrück to the east, residential housing to the north and a small industrial area to the south. The GS extends for $>800\,m$ to the west.

Ballast is used as a collective term for a heterogeneous mix of shattered rock types which are produced mainly for constructive applications, such as stuffing material in road construction or for railway tracks. The Osnabrück ballast layer consists mainly of sandstone, greywacke and diabase. The average thickness of the ballast layer, as estimated by drillings, is around 0.3–1 m. At the measurement site the thickness of the ballast bulk was 0.5 m. Owing to the geometrical heterogeneity of the individual ballast pieces (Fig. 1), it is not easy to accurately estimate their grain size. However, the dimensions of the ballast vary between $2.5\,cm < d < 7.1\,cm$ in diameter and $1.35\,cm < h <$ and $3.5\,cm$ in height which is defined normal to the diameter. The knowledge of further properties of the ballast is important in order to estimate the volumetric heat capacity which in turn is needed to calculate the heat storage Q_S. The porosity of the ballast bulk defined as the ratio of the volume of air-filled cavities to the entire bulk volume (e.g. Marshall et al., 1999) was estimated by adding water to a fixed amount of ballast in a measurement box (Asaeda et al., 1996). The magnitudes of the ballast bulk properties are given in Table 1.

Fig. 1. Ballast surface at the study site in Osnabrück

Table 1. Ballast physical and thermal properties

Porosity	0.45
Bulk density	$1500\,kg\,m^{-3}$
Damping depth	0.09 m
Thermal conductivity	$0.45\,W\,m^{-1}\,K^{-1}$
Thermal diffusivity	$0.32 \cdot 10^{-6}\,m^2\,s^{-1}$
Volumetric heat capacity	$1.39 \cdot 10^{6}\,J\,m^{-3}\,K^{-1}$

3.2 Instrumentation

From 12 June to 23 September 2002 an energy-balance station was installed at GS to measure net radiation Q^*, the turbulent sensible and latent heat fluxes Q_H and Q_E, ground heat flux Q_G and soil temperatures. Q^* was measured by a Pyrradiometer (Ph. Schenk, Vienna, Austria) at 2 m above ground level (a.g.l.). The turbulent sensible (Q_H) and latent (Q_E) heat fluxes were determined by a modified Bowen-ratio method (Liu and Foken, 2001) using a USA-1 sonic anemometer sampling at 2.1 m a.g.l. with 10 Hz (Metek, Schenefeld, Germany) and dry- and wet-bulb temperatures at 0.45 m and 2.05 m a.g.l. (Thies Clima, Göttingen, Germany, with glass-coated PT 100's). The modified Bowen-ratio estimates Q_H from buoyancy flux measurements which are corrected for humidity and cross-wind fluctuations (Liu et al., 2001). Finally, Q_E is calculated

$$Q_E = \frac{Q_H}{Bo} \quad (4)$$

with Q_E and Q_H the latent and turbulent heat flux density in $W\,m^{-2}$ and Bo the Bowen-ratio. Bo was calculated from temperature and humidity measurements at two levels above ground. For a detailed description of the method see Liu and Foken (2001). To ensure good data quality, restrictive criteria are proposed for the modified Bowen-ratio to exclude data during poorly developed turbulent conditions. According to the proposed data-quality criteria (Liu and Foken, 2001) 30 min averages with friction velocity $u_* < 0.07\,m\,s^{-1}$, kinematic heat fluxes $-0.001\,K\,m\,s^{-1} < \overline{w'T'} < 0.002\,K\,m\,s^{-1}$ and Bowen ratios $-0.2 < Bo < 0.05$ were excluded from the data-set.

To measure the heat flux into the ground, a soil heat flux plate was placed at -0.05 m within the ballast bulk (Huskeflux HFP 01, Delft, Netherlands (depths are defined as negative away from the surface)). The circular HFP has a diameter of 8 cm with a temperature sensitive area of about 2 cm in diameter. To insure best possible contact between substrate and HFP, the ballast pieces next to the HFP were sawn in half and the flat sides placed directly in contact with the temperature sensitive part above and below the HFP. Although the complete surface of the HFP was covered by the ballast pieces there are still fractions of the surface which are in contact with pore air owing to the large grain size and complex geometry of the ballast. A thermistor profile was installed at -0.05 m, -0.1 m and -0.3 (Thies Clima, Göttingen, Germany) within the ballast layer. As for the HFP, the thermistors were placed in such a way that parts were in contact with the ballast as well as in contact with pore air to obtain representative data on the thermal structure within the ballast bulk. The thermistors have been tested against each other prior to the field campaign and were found to deviate < 0.05 K.

Net radiation, soil temperatures, soil heat flux and dry- and wet-bulb temperatures were sampled at 1 Hz and stored as 3 min averages to a datalogger Combilog 1020 (Th. Friedrichs, Schenefeld, Germany). From the raw sonic data half hourly fluxes of Q_H and Q_E were calculated using software developed by the Department of Micrometeorology, University of Bayreuth, Germany (Foken, 1999).

To verify the performance of a modelled ballast surface temperature (cf. Section 3.4) these were compared to temperature measurements taken with a handheld infrared thermometer (I-Tec 2003, Novasens, Lüneburg, Germany).

Most of the data presented here were gathered during high-pressure atmospheric conditions, defined as clear and calm days, during which urban climatic effects are most pronounced. Such days are characterised by high shortwave radiative input and are mainly non-overcast during day and night. A description of the classification of these situations is given in Weber and Kuttler (2004).

3.3 Methods to calculate the ground heat flux

For this research four different methods for calculating the heat flux into the ground were taken into account: a combination method with a heat flux plate (-0.05 m) and the correction for heat storage above the HFP from the temperature measurement at -0.05 m and the modelled surface temperature (Q_GHFP); a combination method with a temperature gradient approach with temperature measurements at -0.05 m and -0.1 m below ground level with the correction for heat storage above that layer from the temperature measurement at -0.05 m and the modelled surface temperature (Q_GTG); a temperature gradient approach from a modelled surface temperature (cf. Section 3.4) and temperature measurements at -0.05 m (Q_G0); a residual method ($Q_G$res) as calculated from the surface energy balance equation

$$Q_G\text{res} = Q^* - Q_H - Q_E \qquad (5)$$

with Q^* the net radiation in $W\,m^{-2}$. For all methods, 30 min averages of the ground heat flux were determined (see Table 2 for a summary of the four methods).

Due to the turbulence measurements quality criteria (cf. Section 3.2) some energy balance estimates could not be calculated. Although data gaps are generally limited to a few night-time hours due to low friction velocity conditions below the threshold value of $0.07\,m\,s^{-1}$, some daytime estimates, especially during the morning and evening periods, are unavailable. However, data availability during clear and calm days

Table 2. Overview of the different approaches to calculate the ground heat flux within the porous urban ballast layer in Osnabrück

Method	Approach	Calculation	Needed parameters
Q_GHFP	combination	Q_GHFP[a] + Q_S[b]	HFP (−0.05 m); C_v; T_0; T-0,05 m; z
Q_GTG	combination	Q_GTG[c] + Q_S[b]	T (−0.05; −0.1 m); C_v; T_0; T-0,05 m; z
Q_G0	gradient	see Eq. (1)	T (T_0; −0.05 m); λ; z
$Q_G$res	residual	see Eq. (5)	Q^*; Q_H; Q_E

[a] Heat flux plate measurements not corrected for heat storage (cf. Section 4.1)
[b] For calculation of Q_S see Eq. (3)
[c] Temperature gradient measurements not corrected for heat storage (cf. Section 4.1)

was on average >70%. Gaps in the $Q_G$res time series were filled by linear interpolation between the available $Q_G$res data points.

In the combination methods Q_GHFP and Q_GTG, the heat storage was evaluated according to Eq. (3). The layer averaged temperature was computed from the temperature measurement at −0.05 m and the surface temperature T_0 (cf. Section 3.4). The volumetric heat capacity C_v was calculated from

$$C_v = \frac{\lambda}{\alpha} \tag{6}$$

with α the thermal diffusivity in $m^2\,s^{-1}$. The thermal conductivity of the ballast in Osnabrück was estimated by a laboratory set-up in which the ballast together with a reference material (Agar-gel) was placed in two layers in a measurement box between a hot (at the top) and a cold (at the bottom) plate (for details see Weber, 2004). With the known thermal properties of the reference material and additional temperature measurements across the measurement volume, the thermal conductivity can easily be calculated from the Fourier law of heat conduction. The thermal diffusivity was calculated on a daily basis by the amplitude equation with in-situ temperature measurements at −0.05 m and −0.1 m (Verhoef et al., 1996).

The thermal conductivity of the ballast layer was derived by a laboratory experiment and can be regarded as an effective thermal conductivity taking into account heat transfer through large pore spaces. It was estimated with $\lambda = 0.45\,W\,m^{-1}\,K^{-1}$ with an accuracy of ±7% (Weber, 2004). The thermal diffusivity was calculated according to the amplitude equation (Verhoef et al., 1996) with $\alpha = 0.32 \cdot 10^{-6}\,m^2\,s^{-1}$, which results in a damping depth of about 0.09 m.

Table 3. Overview of thermal properties (λ and C_v) of familiar urban surface materials after Oke (1987) and Zmarsly et al. (2002). The value in brackets indicates the ratio of the thermal property of the relevant material to that of the ballast bulk. The ballast values emanate from the present study

Material	Thermal conductivity λ [$W\,m^{-1}\,K^{-1}$]	Volumetric heat capacity C_v [$J\,m^{-3}\,K^{-1}$]
Asphalt	0.75 (1.67)	$1.94 \cdot 10^6$ (1.41)
Concrete	4.6 (10.23)	$2.2 \cdot 10^6$ (1.59)
Glass	0.74 (1.64)	$1.66 \cdot 10^6$ (1.20)
Stone	2.19 (4.87)	$2.25 \cdot 10^6$ (1.63)
Steel	53.3 (118.45)	$3.93 \cdot 10^6$ (2.84)
Ballast	0.45 (1)	$1.39 \cdot 10^6$ (1)

To account for heat storage in the combination methods Q_GHFP and Q_GTG, the volumetric heat capacity for ballast was calculated according to Eq. (6). Due to the ballast-composition of two materials (air and stone) with quite different thermal properties in terms of λ and C_v, the ballast bulk shows generally smaller magnitudes in comparison to the thermal properties of familiar urban surface materials (Table 3) such as asphalt, stone or dense concrete (Oke, 1987; Zmarsly et al., 2002). For instance, the ratios of thermal conductivity of common urban surface materials to that of ballast ranging from 1.64 to 118.45, the ratios calculated for C_v range from 1.20 to 2.84.

3.4 Modelling the ballast surface temperature

Owing to the dimensions of the individual ballast pieces and the surface conditions of the ballast layer, the surface temperature (T_0) was not measured by in-situ sensors. T_0 was calculated from the longwave radiation at the surface (assuming the longwave emissivity $\varepsilon = 0.99$) which was

modelled according to Sozzi et al. (1999). The method which is straightforward and only needs standard meteorological data will be briefly summarised here. It is based on the Stefan-Boltzmann law plus an additional term

$$L\uparrow_{mod} = \varepsilon \cdot \sigma \cdot T_{av}{}^4 + c \cdot Q^* \quad (7)$$

with $L\uparrow_{mod}$ the modelled upward longwave radiation in $W\,m^{-2}$, ε longwave emissivity, σ Stefan-Boltzmann's constant in $W\,m^{-2}\,K^{-4}$, T_{av} an average of the air temperature at 0.45 m a.g.l. and the ground temperature at -0.05 m in K, c the heating coefficient and Q^* net radiation in $W\,m^{-2}$.

Inserting near surface air temperature measurements in Eq. (7) can only give a rough estimate of the real surface temperature. Therefore, the term $c \cdot Q^*$ is incorporated and aims to virtually extrapolate the temperature profile down to the ground surface to give the amount of radiative input absorbed at the surface defining the "real" surface temperature.

To estimate the magnitude of c, the best linear fit between the modelled T_0 (T_0 mod) and the nocturnal measurements of $L\uparrow$ by the Pyrradiometer converted into surface temperature (T_0 Pyr.) was approximated with different values for c. The best fit with only little deviation between the data-sets ($R^2 = 0.99$) was obtained for $c = 0.18$ (Fig. 2). The accuracy of T_0 mod in comparison to T_0 Pyr. is satisfying with a standard error of deviation of 0.45 K in the given temperature range from 10 °C to 30 °C. Comparison of T_0 mod with temporary measurements taken using a handheld infrared thermometer ($T_{0\,IR}$) showed good agreement for data during both, day and night (Fig. 3).

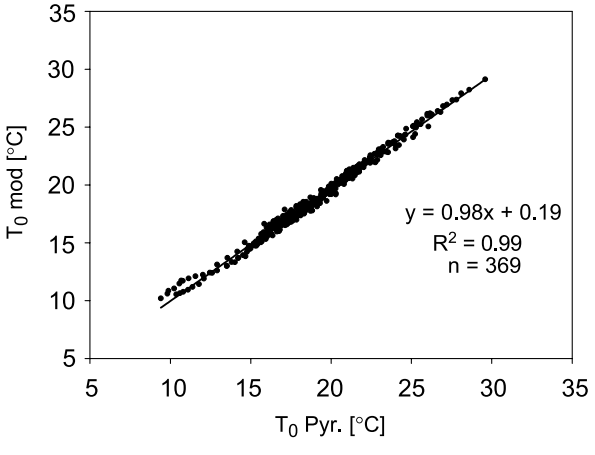

Fig. 2. Scatter plot of the modelled surface temperature (T_0) and the measured nocturnal upward longwave radiation converted to surface temperature (T_0 Pyr.). The heating coefficient c is set to $c = 0.18$ (cf. Eq. (7)). The regression is based on 369 nocturnal 30 min averages during clear and calm nights during the study period from 12 June–23 September 2002

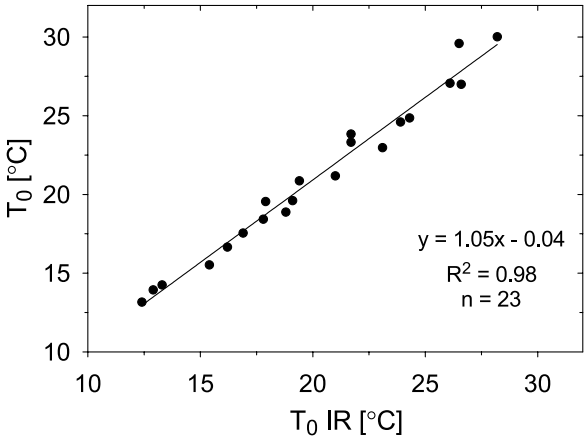

Fig. 3. Scatter plot of the modelled surface temperature (T_0) and the surface temperature as measured temporary by infrared-thermometry ($T_{0\,IR}$) during the study period from 12 June–23 September 2002

4. Results

4.1 Performance of the HFP

First of all, the measurement performance between the ground heat flux calculated from the laboratory derived thermal conductivity by the temperature gradient approach (Q_GTG, Eq. (1)), and the ground heat flux as estimated by the heat flux plate (Q_GHFP) will be compared. Therefore, both methods are not corrected for heat storage at this stage. A geometrical shape correction for the HFP, the so-called Philips-correction (Philip, 1961) was not applied since it remains a source of controversy within the literature and has also been shown to be of minor influence on the data (~5%). As indicated in Fig. 4, Q_GHFP is underestimated by about 26% in comparison to the temperature gradient. This fact is especially interesting because Q_GTG is calculated from a substrate layer centred at -0.075 m (temperature gradient between -0.05 m and -0.1 m) which is 2.5 cm below the depth of the HFP. With an accurate performance of the HFP one would consider the heat flux to be greater in magnitude compared to the

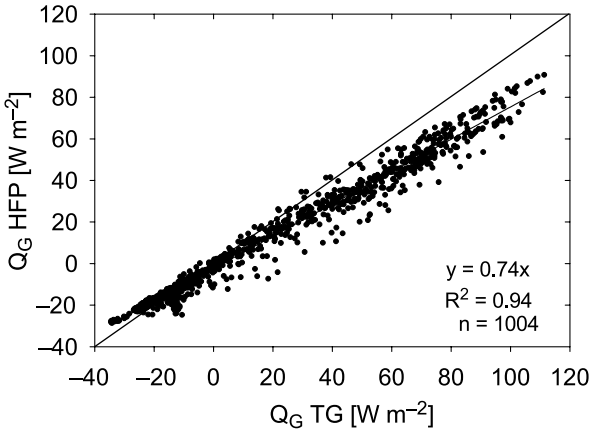

Fig. 4. Scatter plot of the ground heat flux as derived by the temperature gradient between −0.05 and −0.1 m (Q_GTG) vs. the heat flux plate measurements at −0.05 m (Q_GHFP). The regression is based on 1004 30 min averages during clear and calm days in the study period from 12 June–23 September 2002. They dashed line indicates the 1:1 line

temperature gradient because of heat flux divergence within the uppermost centimetres of the ballast bulk. The underestimation of Q_GHFP is believed to be mainly attributed to poor contact between the individual ballast pieces and the HFP although sawn ballast pieces have been introduced to enhance contact (cf. Section 3.2). Just a thin layer of air between the HFP and the ballast shifts the measurements towards the material with a considerably smaller thermal conductivity. The air acts as an insulating layer, decreasing the magnitude of Q_G.

4.2 Comparison of methods to estimate Q_G

In this section, the ground heat fluxes as calculated from the combination methods (Q_GHFP, Q_GTG) are compared to the temperature gradient method (Q_G0) and the residual method ($Q_G$res), with respect to differences in absolute values as well as temporal variability over the course of the day.

During the times of highest radiative input, during the morning and noon periods, the combination methods are larger than Q_G0. Summed over the diurnal course this amounts to 23% and 31%, respectively, for a single clear and calm day (29 July, 2002), while on average the combination methods are 17% and 27% larger when compared to Q_G0 (Table 4).

The time dependent behaviour of the time series are comparable during the morning hours

Table 4. Daily sums of the ground heat flux in MJ m^{-2} d^{-1} calculated for different methods on 29 July, 2002 and for the daily average sums for 21 clear and calm days during the study period from 12 June 2002 to 23 September 2002. For both cases, the ratio of the relevant method (Q_G(i)) to the method Q_G0 is indicated

	Sum 29 July 2002	$Q_G(i)/Q_G0$	Average sum	$Q_G(i)/Q_G0$
Q_GHFP	5.48	1.23	4.40	1.17
Q_GTG	5.81	1.31	4.79	1.27
Q_G0	4.45	1	3.77	1
$Q_G$res	11.25	2.53	9.44	2.50

with relatively small deviations of, on average, 5–20 W m^{-2}, both for a single clear and calm day (Fig. 5a) as well as for an average of 21 clear

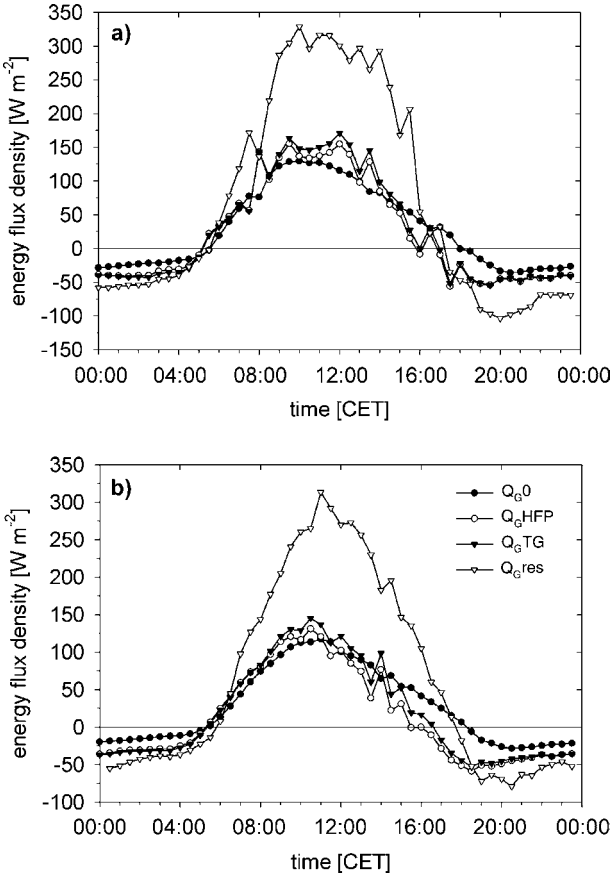

Fig. 5. Plots of the ground heat fluxes estimated from temperature gradients between the surface and −0.05 m (Q_G0), the combination methods with heat flux plate data (Q_GHFP) and temperature gradients (Q_GTG) and as residual term of the energy-balance-equation ($Q_G$res). For the clear and calm day 29 July, 2002 (**a**) and averages for 21 clear and calm days in the study period from 12 June–23 September 2002 (**b**)

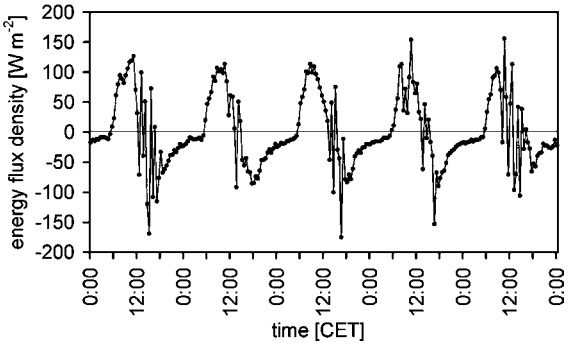

Fig. 6. Heat storage Q_S in the layer between the surface and −0.05 m for a five-day period from 15–19 August, 2002

and calm days (Fig. 5b). During the afternoon and evening period however, deviations between the methods become significant and are in the range 20–40 W m^{-2}. Occasionally, deviations are as large as 60 W m^{-2} (17:30 CET, see Fig. 5b). The combination method time series decreases faster in comparison to the Q_G0 time series. This is due to the important influence of the heat storage term Q_S on the ground heat fluxes calculated from the combination methods.

To analyse the behaviour of the combination methods the heat storage time series Q_S is plotted in Fig. 6 for a five-day period during clear and calm weather. It is evident that the storage term Q_S is far greater in magnitude, as are the ground heat fluxes (over the diurnal course on 29 July, 2002 the heat storage term Q_S accounts for 78% of Q_GHFP and for 74% of Q_GTG). Owing to the time rate of change of temperature in the layer between the surface, and the temperature (or HFP) measurement, respectively, heat storage strongly increases during the morning hours due to increasing surface temperatures (cf. Eq. (3)). After the surface temperature peaks around noon, Q_S decreases rapidly and varies strongly. The storage term reaches negative values of up to −150 W m^{-2} (Fig. 6). This is due to the different cooling rates of the surface temperature and the temperature measurement at −0.05 m. The time rate of change in temperature of the upper 5 cm of the ballast bulk becomes negative – and so does the storage term Q_S. Due to the stronger cooling of the surface during two consecutive 30 min time steps, the resulting storage term might reach large values which are physically implausible on such short time scales. It has to be noted that due to the approach of modelling the surface temperature by the upward longwave radiation at the surface (Eq. (7)), time rates of change in surface temperatures might sometimes be biased by meteorological conditions (shading etc.) on short time scales. As a consequence, the magnitude of the fluxes, Q_GHFP and Q_GTG, are strongly influenced by the time series of Q_S.

The estimates of the residual term ($Q_G$res) are by far the largest ground heat fluxes of all methods not only for 29 July 2002 but also for the 21-day average. The daily sum of $Q_G$res exceeds the gradient method Q_G0 by a factor of, on average, 2.5 (Table 4). Absolute differences between $Q_G$res and Q_G0 on the diurnal cycle amount to 200 W m^{-2} at 10:00 CET on the 29 July 2002 (Fig. 5a) or to 147 W m^{-2} at 10:00 CET when averaged over 21 days (Fig. 5b). It is also evident that absolute differences are largest at times of highest energy input, i.e. during noon-hours. This indicates some sort of systematic underestimation of energy conversion in one of the fluxes measured at the energy balance site although all terms were tested and were found to have been measured accurately. Consequences for the estimation of urban ground heat fluxes from a residual approach will be briefly discussed in the following section.

5. Discussion of results

Given the variability between the different ground heat fluxes estimated for the porous ballast layer in Osnabrück, which is now the most suitable method?

As already mentioned, no standard exists as e.g. in homogeneous fine-textured soils where the heat flux plate has been proven to be reliable and is currently the quasi-standard of soil heat flux measurements. This is why a relative comparison between the different methods has to be considered in this study.

In the combination methods Q_GHFP and Q_GTG, as well as in the residual method $Q_G$res, large errors have to be taken into account (cf. Section 4.2). In the combination methods, the inaccuracies are largely tied to the dynamic behaviour of the heat storage term Q_S triggered by the variation in the warming of the upper centimetres of the ballast bulk on the daily cycle (cf. Section 4.2). The accuracy of the residual method is closely tied to

uncertainties in the estimation of the surface-energy-balance. The non-closure of the surface-energy-balance showed a magnitude of about 30% at the study site in Osnabrück (Weber, 2004). This value is plausible considering the heterogeneity of the site within the urban environment. Even studies that were performed at flat and homogeneous study sites, with state-of-the-art measurement equipment, reported gaps in the energy balance closure of 10–40% (Panin et al., 1998; Oncley et al., 2002; Wilson et al., 2002). As a consequence, the residual estimation of the ground heat flux is barely reliable at study sites exhibiting a certain degree of heterogeneity. As a result, the estimation of the ground heat flux using a residual approach is only feasible with a nearly perfect closure of the energy balance, although large random errors on short time scales might still occur.

Having this in mind, the gradient approach Q_G0 gives the most plausible results in this study. This is not only valid for the absolute values, but also for the temporal dynamics of the ground heat flux on the diurnal cycle. The accuracy of the gradient method Q_G0 basically depends on the temperature gradient measurements in the substrate. The in-situ measurements with the thermistor profile can be achieved with a high degree of accuracy (cf. Section 3.2). The main limitations in this approach are inaccuracies in the modelled surface temperature and the measurement depth within the substrate owing to the large grain size distribution of the ballast. Although the modelled surface temperature has shown reliable results (cf. Fig. 3) errors might be introduced due to steep gradients of temperature near the surface. To give an assessment of the performance of the method the relative error of Q_G0 can be written as (Taylor, 1988)

$$\frac{\delta(Q_G0)}{|Q_G0|} = \sqrt{\left(\frac{\delta\lambda}{|\lambda|}\right)^2 + \left(\frac{\delta T}{|T|}\right)^2 + \left(\frac{\delta z}{|z|}\right)^2} \tag{8}$$

with $\delta x/|x|$ representing the relative errors of the independent input variables. With the known error $\lambda \sim 7\%$, an assumed maximum error of $T_0 \sim 1\,K$ for the surface temperature and an error associated with the measuring depth of 0.01 m, the error of Q_G0 at a typical noon situation ($\Delta T = 10\,K$) would result in 23%.

Using Eq. (8) the relative errors of the other methods can be roughly estimated. Again, some assumptions about the partial error contributing to the overall error for each method have to be made which are assumed to mark an upper uncertainty limit. These are 20% for measurements with the HFP (according to the manufacturer), 7% for C_v (due to the error on λ in Eq. (6)), 10% for Q^* (see discussion in Weber, 2004), and 10% and 20% for Q_H and Q_E, respectively (accuracy limits for the modified Bowen ratio given by Liu and Foken, 2001). As a consequence, relative errors for the methods are about 31% for Q_GHFP, 33% for Q_GTG and 38% for $Q_G$res.

With a relative error of 23%, the inaccuracy of Q_G0 is non-negligible. But in comparison to the other methods Q_G0 incorporates the smallest uncertainties and leads to far more plausible results.

6. Concluding remarks

The ground heat flux in a porous urban ballast layer was calculated using four different methods. The methods showed distinct differences in absolute magnitudes of the ground heat fluxes as well as in temporal dynamics associated with the penetration of the diurnal temperature wave into the ground. The results of this study indicate that the method which calculates the ground heat flux by the Fourier law of heat conduction taking the effective thermal conductivity, a modelled surface temperature and temperature measurements at -0.05 m below the surface into account (Q_G0) yields the most plausible results.

Nevertheless more research and data are needed to compare methods to find reliable ways to determine ground heat fluxes accurately within urban environments in the future.

References

Al-Turki AM, Gari HN, Zaki GM (1997) Comparative study on reduction of cooling loads by roof gravel cover. Energ Buildings 25(1): 1–5

Anandakumar K (1999) A study on the partition of net radiation into heat fluxes on a dry asphalt surface. Atmos Environ 33: 3911–3918

Arya PS (2001) Introduction to micrometeorology. International Geophysics Series, 42. San Diego: Academic Press, 304 pp

Asaeda T, Ca VT, Wake A (1996) Heat storage of pavement and its effect on the lower atmosphere. Atmos Environ 30(3): 413–427

Christen A, Vogt R (2004) Energy and radiation balance of a central European city. Int J Climatol 24: 1395–1421

Doll D, Ching JKS, Kaneshiro J (1985) Parameterization of subsurface heating for soil and concrete using net radiation data. Bound-Layer Meteorol 32: 351–372

Foken T (1999) Der Bayreuther Turbulenzknecht, Arbeitsergebnisse, Universität Bayreuth, Abt. Mikrometeorologie, Print ISSN 1614-8916, No. 1, 16 pp

Grimmond CSB, Oke TR (1999) Heat storage in urban areas: Local scale observations and evaluation of a simple model. J Appl Meteor 38: 922–940

Grimmond CSB, Oke TR (2002) Turbulent heat fluxes in urban areas: Observations and a local-scale urban meteorological parameterization scheme (LUMPS). J Appl Meteor 41: 792–810

Heusinkveld BG, Jacobs AFG, Holtslag AAM, Berkowicz SM (2003) Surface energy balance closure in an arid region: role of soil heat flux. Agric Forest Meteorol 122(1–2): 21–37

Jauregui E, Moreno MC, Tejeda A (2002) The energy balance of central Barcelona, Fourth Symposium on the Urban Environment, American Meteorological Society, 20. – 24.05.2002, Norfolk, Paper 9.6, 3 S

Kukharets VP, Perepelkin VG, Tsvang LR, Richter SH, Weisensee U, Foken T (1998) Energiebilanz an der Erdoberfläche und Wärmespeicherung im Boden. In: Foken T (ed) Ergebnisse des LINEX-97/1 Experimentes. Arbeitsergebnisse Nr. 53. Deutscher Wetterdienst DWD, Offenbach a. M., 38 pp

Liu H, Foken T (2001) A modified Bowen-ratio method to determine sensible and latent heat fluxes. Meteorol Z 10(1): 71–80

Liu H, Peters G, Foken T (2001) New equations for sonic temperature variance and buoancy heat flux with an omnidirectional sonic anemometer. Bound-Layer Meteorol 100: 459–468

Marshall TJ, Holmes JW, Rose CW (1999) Soil physics. Cambridge: Cambridge University Press, 453 pp

Masson V, Grimmond CSB, Oke TR (2002) Evaluation of the Town Energy Balance (TEB) scheme with direct measurements from dry districts in two cities. J Appl Meteor 41(10): 1011–1026

Mayocchi CL, Bristow KL (1995) Soil surface heat flux: some general questions and comments on measurements. Agric Forest Meteorol 75(1–3): 43–50

Mogensen OV (1970) The calibration factor in heat flux meters in relation to the thermal conductivity of the surrounding medium. Agric Forest Meteorol 7: 401–410

Munn RE (1966) Descriptive micrometeorology. Advances in Geophysics. London: Academic Press, 245 pp

Oke TR (1987) Boundary layer climates. Methuen, London: 2nd edn., 435 pp

Oke TR (1988) The urban energy balance. Prog Phys Geog 12(1): 471–508

Oke TR, Spronken-Smith RA, Jauregui E, Grimmond CSB (1999) The energy balance of central Mexico City during the dry season. Atmos Environ 33: 3919–3930

Oncley S, Foken T, Vogt R, Bernhofer C, Kohsiek W, Liu H, Pitacco A, Grantz D, Riberio L, Weidinger T (2002) The energy balance experiment EBEX 2000. In: AMS (ed) 25th Conference Agricultural and Forest Meteorology, Norfolk, pp 1–2

Panin GN, Tetzlaff G, Raabe A (1998) Inhomogeneity of the land surface and problems in the parameterization of surface fluxes in natural conditions. Theor Appl Climatol 60: 163–178

Passerat de Silans A, Monteney BA, Lhomme JP (1997) The correction of soil heat flux measurements to derive an accurate surface energy balance by the Bowen ratio method. J Hydrol 188–189(1–4): 453–465

Philip JR (1961) The theory of heat flux meters. J Geophys Res 66(2): 571–579

Roberts SM, Oke TR, Voogt JA, Grimmond CSB, Lemonsu A (2003) Energy storage in a european city center, Fifth International Conference on Urban Climate, 01.-05.09.2003, Lodz, Poland, pp 241–244

Roth M, Oke TR (1994) Comparison of modelled and measured heat storage in suburban terrain. Beitr Phys Atmos 67(2): 149–156

Sauer TJ (2002) Heat flux density. In: Dane JH, Topp GC (eds) Methods of soil analysis. Part 4 Physical Methods. SSSA, Madison, pp 1233–1248

Sauer TJ, Meek DW, Ochsner TE, Harris AR, Horton R (2003) Errors in heat flux measurement by flux plates of contrasting design and thermal conductivity. Vadose Zone Journal(2): 580–588

Schotanus P, Nieuwstadt FTM, de Bruin HAR (1983) Temperature measurement with a sonic anemometer and its application to heat and moisture fluxes. Bound-Layer Meteorol 26: 81–93

Sozzi R, Salcido A, Flores RS, Georgiadis T (1999) Daytime net radiation parameterisation for Mexico City suburban areas. Atmos Res 50: 53–68

Spronken-Smith R (2002) Comparison of summer and winter-time suburban energy fluxes in Christchurch, New Zealand. Int J Climatol 22(8): 979–992

Taylor J (1988) Fehleranalyse. Weinheim, Basel, Cambridge, New York: VCH-Verlag, 243 pp

van Loon WKP, Bastings HMH, Moors EJ (1998) Calibration of soil heat flux sensors. Agric Forest Meteorol 92(1): 1–8

Verhoef A, van den Hurk BJJM, Jacobs AFG, Heusinkveld BG (1996) Thermal soil properties for vineyard (EFEDA-I) and savanna (HAPEX-Sahel) sites. Agric Forest Meteorol 78(1–2): 1–18

Watts DB, Kanemasu ET, Tanner CB (1990) Modified heat-meter method for determining soil heat flux. Agric Forest Meteorol 49: 311–330

Weber S (2004) Energiebilanz und Kaltluftdynamik einer urbanen Luftleitbahn. Essener Ökologische Schriften Band 21, Westarp Wissenschaften, Hohenwarsleben, 203 S

Weber S, Kuttler W (2003) Analyse der nächtlichen Kaltluftdynamik und -qualität einer stadtklimarelevanten Luftleitbahn. Gefahrstoffe – Reinhaltung der Luft 63(9): 381–386

Weber S, Kuttler W (2004) Cold-air ventilation and the nocturnal boundary layer structure above an urban ballast facet. Meteorol Z 13(5): 405–412

Wilson K, Goldstein A, Falge E, Aubinet M, Baldocchi D, Berbigier P, Bernhofer C, Ceulemans R, Dolman H, Field C, Grelle A, Ibrom A, Law BE, Kowalski A, Meyers TP, Monson R, Oechel W, Tenhunen J, Valentini R, Verma SB (2002) Energy balance closure at FLUXNET sites. Agric Forest Meteorol 113(1–4): 223–243

Zmarsly E, Kuttler W, Pethe H (2002) Meteorologisch – klimatologisches Grundwissen, 2nd edn. Stuttgart: Eugen Ulmer Verlag, 174 pp

Author's address: Stephan Weber (e-mail: stephan.weber@uni-essen.de), Department of Applied Climatology and Landscape Ecology, Institute of Geography, University of Duisburg-Essen, Campus Essen, Universitätsstrasse 5, 45141 Essen, Germany.